Hydrogenation of calcite and change in chemical bonding at high pressure: diamond formation above 100 GPa

Alexander F. Goncharov[1], Huiyao Kuang [2], John S. Tse [2], Eric Edmund [1], Maxim Bykov [3,4], Elena Bykova [5], Stella Chariton [6], Vitali B. Prakapenka [6], Timofey Fedotenko [7], Nico Giordano[7], Mohamed Mezouar [8], Jesse S. Smith [9]

[1] Earth and Planets Laboratory, Carnegie Institution for Science, Washington, DC 20015, USA

[2] Department of Physics and Engineering Physics, University of Saskatchewan, Saskatoon, Canada

[3] Institute of Inorganic Chemistry, University of Cologne, Greinstrasse 6, 50939 Cologne, Germany

[4] Institute of Inorganic and Analytical Chemistry, Johann Wolfgang Goethe Universität Frankfurt, Max-von-Laue-Straße 7, D-60438 Frankfurt am Main, Germany

[5] Goethe-Universität Frankfurt am Main, Facheinheit Mineralogie, 60438 Frankfurt am Main, Germany

[6] Center for Advanced Radiation Sources, University of Chicago, Lemont, IL 60637, USA

[7] Deutsches Elektronen-Synchrotron DESY, Notkestr. 85, 22607 Hamburg, Germany

[8] European Synchrotron Radiation Facility BP 220, 38043 Grenoble Cedex, France

[9] HPCAT, X-ray Science Division, Argonne National Laboratory, Argonne, Illinois 60439, USA

Synchrotron X-ray diffraction (XRD) and Raman spectroscopy in laser heated diamond anvil cells and first principles molecular dynamics (FPMD) calculations have been used to investigate the reactivity of calcite and molecular hydrogen (H_2) at high pressures up to 120 GPa. We find that hydrogen reacts with calcite starting below 0.5 GPa at room temperature

forming chemical bonds with carbon and oxygen. This results in the unit cell volume expansion; the hydrogenation level is much higher for powdered samples. Single-crystal XRD measurements at 8-24 GPa reveal the presence of previously reported III, IIIb, and VI calcite phases; some crystallites show up to 4% expansion, which is consistent with the incorporation of ≤ 1 hydrogen atom per formula unit. At 40-102 GPa XRD patterns of hydrogenated calcite demonstrate broadened features consistent with the calcite VI structure with incorporated hydrogen atoms. Above 80 GPa, the C-O stretching mode of calcite splits suggesting a change in the coordination of C-O bonds. Laser heating at 110 GPa results in the formation of C-C bonds manifested in the crystallization of diamond recorded by *in situ* XRD at 300 K and 110 GPa and by Raman spectroscopy on recovered samples commenced with C^{13} calcite. We explored several theoretical models, which show that incorporation of atomic hydrogen results in local distortions of CO_3 groups, formation of corner-shared C-O polyhedra, and chemical bonding of H to C and O, which leads to the lattice expansion and vibrational features consistent with the experiments. The experimental and theoretical results support recent reports on tetrahedral C coordination in high-pressure carbonate glasses and suggest a possible source of the origin of ultradeep diamonds.

INTRODUCTION

The transport of hydrogen in minerals and sediments at high pressures is important for the interpretation of the geochemical cycles which extend into Earth's deep interior (Poli and Schmidt, 2002). The subduction of oceanic crust delivers fluids, minerals, and sediments into the mantle (e.g., (Schmidt and Poli, 2014) (Rapp and Watson, 1995)), and dehydration melting of these aggregates drives buoyant C-O-H fluids to resurface underneath the mantle wedge, while remaining solids subduct deeper into the Earth's interior. Knowing the hydrogen storage capacity of the subducted constituent minerals, and mineral chemical interactions with fluid components such as H_2 or H_2O is critically important to understand fluid-rock interactions and the cycling of volatiles in Earth's interior. Calcite ($CaCO_3$) can comprise up to several wt% in subducted basalt, meaning that it is a significant mineral component in subduction zones, and provides a simple end-member carbonate to study hydrogen-carbonate interactions. Molecular H_2 is a component of reduced C-O-H fluids (Bali et al., 2013; Kadik, 2006; Weidendorfer et al., 2020), and so our experiments can be used to better understand the chemical interactions between carbonates and these fluids. Furthermore, recent *ab initio* calculations have reported that carbonates can decompose into hydroxides and diamond in hydrogenated environments at high pressures and temperatures (Kuang and Tse, 2022).

Anhydrous calcite has been extensively studied before (Bayarjargal et al., 2018; Catalli and Williams, 2005; Gavryushkin et al., 2017; Liu et al., 2016; Lobanov et al., 2017; Merlini et al., 2012; Ono et al., 2007; Ono et al., 2005; Pennacchioni et al., 2023; Suito et al., 2001; Zhao et al., 2022) demonstrating a series of phase transformations with pressure and temperature. Each polymorph of $CaCO_3$ below 100 GPa (e.g., post-aragonite (Yao et al., 2018)) consists of sp^2 -hybridized carbon, forming triangular CO_3^- carbonate groups. At higher pressure carbon is expected to become sp^3 -hybridized. Accordingly, theoretical structure searches discovered two high-pressure phases with infinite chains of CO_4 tetrahedra (Oganov et al., 2006; Pickard and Needs, 2015), which were later reported experimentally (Lobanov et al., 2017; Ono et al., 2007). Recent first-principles theoretical calculations demonstrate that calcium carbonate melt reacts with hydrogen at the Earth's lower mantle conditions, forming various transient chemical species including C-C bonds suggesting possible diamond crystallization (Kuang and Tse, 2022).

Investigations of calcite in hydrous conditions up to 12 GPa and 400 °C do not report incorporation of water in the crystals based on Raman and infrared (IR) results in recovered samples, and also no structural difference compared to the behavior of anhydrous crystals has been reported (Zhao et al., 2022).

Here, we report on the experimental XRD and Raman investigation of calcite which has been saturated and temperature annealed in an H_2 medium at high pressures up to 110 GPa. We find that H_2 incorporates in the calcite lattice in an atomic form at room temperature starting from the lowest pressure studied, demonstrated by the lattice expansion and appearance of the Raman C(O)-H bonds. Above 80 GPa, XRD peaks broaden, while Raman spectra show the appearance of new C-O stretching modes manifesting changes in the C-O bonds related to a partial sp^3 hybridization. At above 105 GPa, we detected the formation of diamond crystallites after laser heating, which manifests the formation of C-C bonds. First-principles molecular dynamics (FPMD) calculations show that the incorporation of atomic hydrogen results in chemical bonding of H to C and O and facilitates the formation of corner-shared C-O polyhedral and C-C bonds. These findings suggest a new source of ultradeep diamonds.

METHODS

Experiments were performed in diamond anvil cells (DAC) with 200- and 100-μm culet diameters. Calcite in two physical forms were used. The powdered samples mixed with very fine Au particles were pressed in thin pellets and loaded in the DAC cavity in a rhenium gasket with molecular H_2 using a gas loading at 0.14 GPa. To avoid the anvil damage due to penetration of H_2, we used freshly polished diamond anvils and reduced the heating time. We used microsecond pulsed laser heating where the sample is heated by a sequence of laser pulses, which are sufficiently long to heat the bulk of the sample, while suppressing unwanted chemical reactions (e.g., Ref. (Goncharov et al., 2010)),. Single crystalline samples were cleaved from large calcite single crystals (MTI). Gold particles were used as in-situ pressure calibrants and to absorb the laser radiation in laser heating experiments. In addition, ruby balls were also used to measure pressure in combined Raman and XRD experiments to pressures up to 80 GPa. Calcites with natural carbon isotope composition (Alfa Aesar) and that of 99% ^{13}C isotope composition (Cambridge Isotope Laboratories) were used in different experiments. Synchrotron XRD and Raman experiments were performed concomitantly in several experiments to highest pressures. Powder XRD experiments were performed at ESRF (ID27 (Mezouar et al., 2017)) and APS (GSECARS and HPCAT); similar measurements combined with laser heating were performed at GSECARS (Prakapenka et al., 2008). Single-crystal experiments were performed at the Extreme Conditions Beamline at Petra III (DESY, Hamburg). In these measurements, XRD patterns were taken sequentially while the sample was rotated around a vertical *ω* axis in a range of ±35° with an angular step Δω = 0.5° and an exposure time of 1–5 seconds per frame. Raman experiments were performed at GSECARS (Holtgrewe et al., 2019) and Carnegie Science Laboratory (Lobanov et al., 2013) using single-grating spectrometers with CCD detectors; the spectra were excited with 488 and 532 nm laser wavelengths.

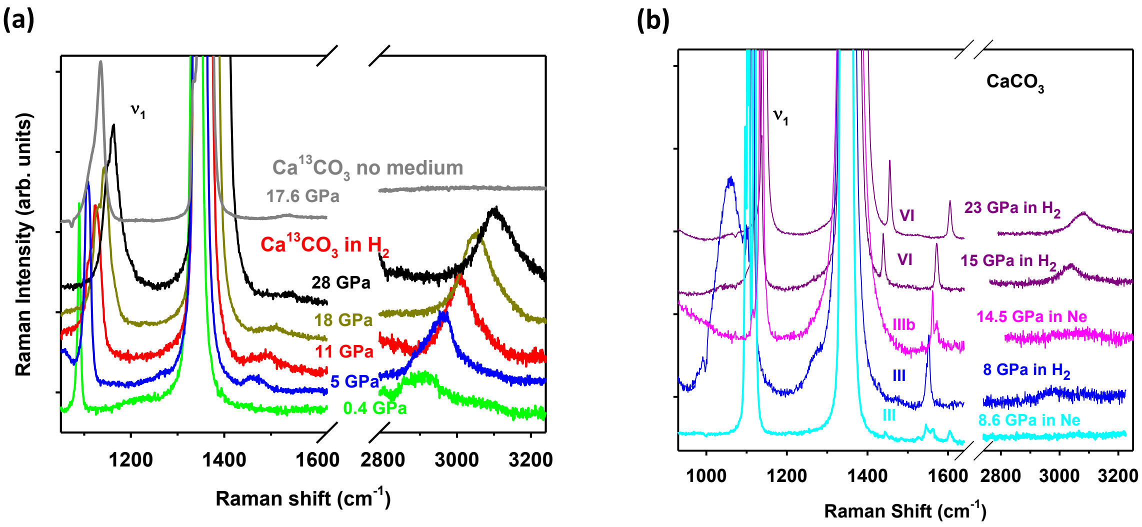

Figure 1. Raman spectra of $Ca^{13}CO_3$ powder pellet (the control spectrum measured without PTM is shown for comparison) (a) and single-crystal $CaCO_3$ (the control spectra measured in Ne PTM is shown for comparison) (b) in H_2 medium measured on pressure increase. The 2900 cm^{-1} band is detected at the lowest pressure in powder experiment after gas-loading of H_2 in a DAC (within 20 minutes at 0.4 GPa, the subsequent spectra are taken in hours to days' time interval), while longer times are needed to hydrogenate single-crystal samples (days to months). The lattice modes of calcite are largely blocked by the rotational excitations of molecular H_2 at 350-1100 cm^{-1} in the powdered sample, but they are well resolved in the single-crystal sample. The Raman spectrum of molecular H_2 is dominated by a strong intramolecular stretching mode at about 4200 cm^{-1}, which does not interfere with hydrogen originated modes reported here. A strong band at 1330-1400 cm^{-1} is due to the stressed diamond anvils.

First-principles molecular dynamics (FPMD) calculations were performed using the Vienna Ab initio Simulation Package (VASP) code Ultrasoft pseudopotentials (US) (42) were used in the simulations. The energy cutoff of the plane-wave basis set was 396 eV. The valence configurations employed in this work are H $1s^1$, C $2s^22p^2$, O $2s^22p^6$, and Ca $3p^64s^2$. Langevin thermostats were used to control the pressure and temperature of the system. Three $CaCO_3$ model structures with different initial H positions and content were used in the simulation. They are all based on a post-aragonite structure with 2 $CaCO_3$ formular units in the unit cell. Model-I started with 4 H atoms attached to C atoms, which are positioned above and below the carbonate ion plane. Model-II had 4 H atoms attached to O atoms in the carbonate plane. Model-III was hydrogen-rich, where 8 H_2 molecules were incorporated in the lattice. The structures were optimized at 48, 66, 78, 90, and 102 GPa.

RESULTS

HYDROGENATION

To characterize the hydrogenation of calcite at pressures below 24 GPa, we combined Raman spectroscopy and single-crystal XRD. From Raman spectroscopy, we found that hydrogen incorporates into the calcite lattice at very low pressures, starting <0.5 GPa. This is evident in the powdered samples from the appearance of a 2900 cm^{-1} band, which increases in intensity with pressure up to 10 GPa (Fig. 1(a)). The vibration frequency of this band increases with pressure indicating the C-H stretch origin as in hydrocarbons (see Ref. (Bykov et al., 2021) and Refs. therein). In addition, we recorded another weaker hard mode near 1450 cm^{-1} (Figs. 1-2). As will be discussed in more detail below, these new Raman bands indicate that hydrogen is incorporated in an atomic form and chemically bonded to calcite. These bands persist to the highest pressures explored (Fig. 2) and exhibit a substantial broadening. Control experiments show that these new bands do not appear in calcite loaded without a pressure-transmitting medium (PTM) or with a Ne PTM (Fig. 1). In comparison, the C(O)-H stretch Raman band at 2900 cm^{-1} is much weaker in single-crystal samples, even after calcite was kept in an H_2 PTM for several months (Fig. 1(b)); a second associated band at 1450 cm^{-1} can also be seen at the level of sensitivity. The intensity of these bands depends on the crystallite: generally, visually clear grains show weaker H-related Raman bands suggesting that H enters the grains that are not optically clear and have internal defects or grain boundaries.

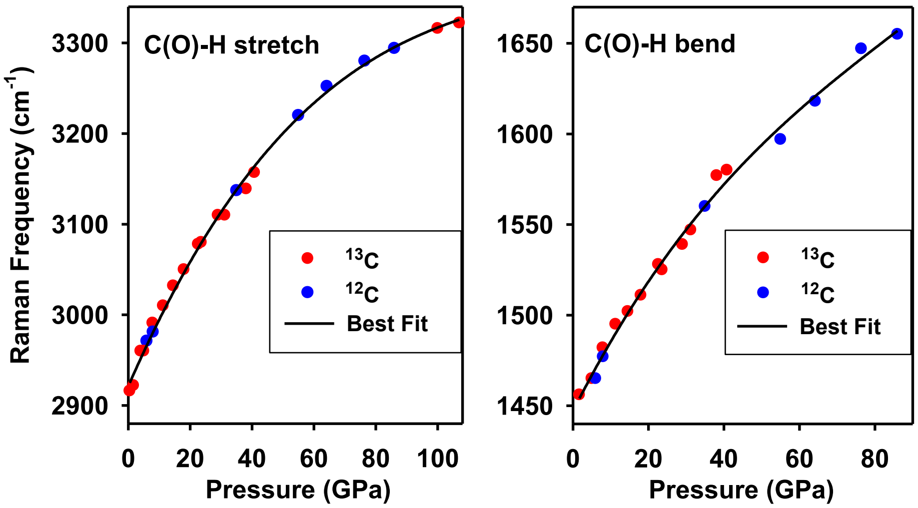

Figure 2. Raman frequencies of the vibrational modes related to the hydrogenation of calcite.

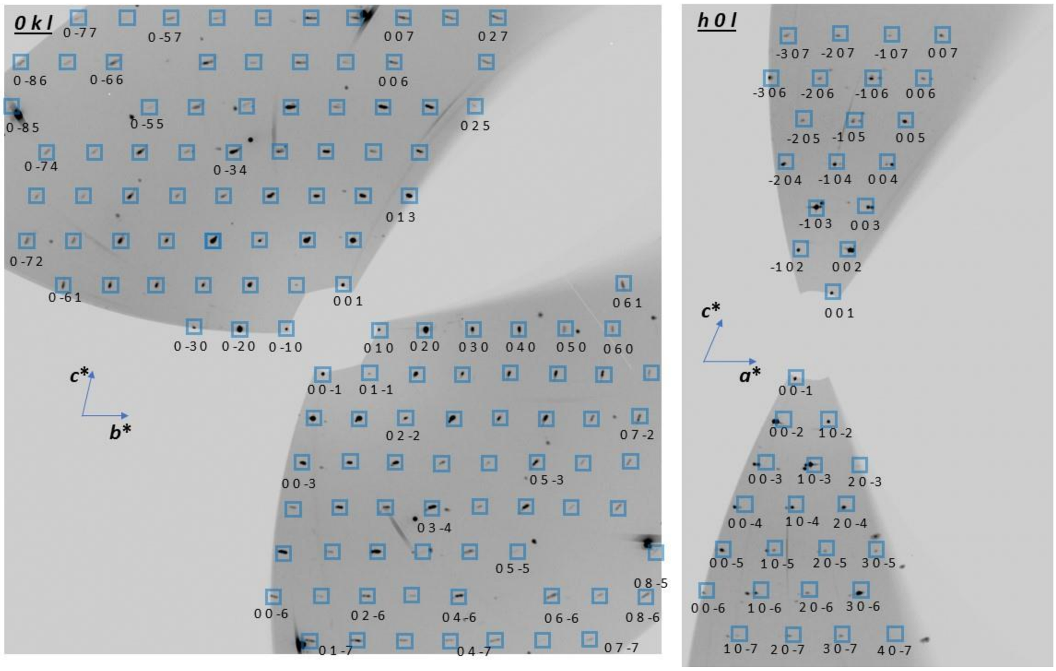

Figure 3. XRD results on single-crystal calcite-VI in H_2 medium at 15 GPa. (a) Reconstructed reciprocal lattice plane defined by various directions. The reflections are framed in blue squares

and *hkl*'s of some reflections are labeled (sufficient to easy assign the unlabeled reflections). The X-ray wavelength is 0.290 Ǻ.

Single-crystal XRD measurements were performed at 8.5, 15, and 23 GPa on the same samples in various sample positions, where the best quality patterns could be collected. The structural information has been determined by applying the technique of multigrain X-ray crystallography to single-crystal samples in DAC (Fig. 3). Up to 20 different crystallites with different orientations and even different structures have been detected and analyzed from the same observation point. These different crystals likely appear due to inhomogeneous stress conditions, inhomogeneous hydrogenation, and phase transformations. At 8 GPa, we found a mixture of calcite-III and calcite-IIIb (Merlini et al., 2012), at 15 GPa we find additional calcite-VI (Merlini et al., 2012) (Fig. 3), and finally, at 24 GPa, there is only calcite-VI. We also measured the same material in identical conditions in a Ne transmitting medium at 14.5 GPa, where calcite-IIIb was found and investigated. In calcite in an H_2 medium, we find that there are crystallites with distinctly different lattice parameters for crystallites of the same symmetry. Such effects were not observed in the control experiment with Ne as a transmitting medium. It is natural to assume that the expanded crystals are due to hydrogen incorporation consistently with Raman observations, described above.

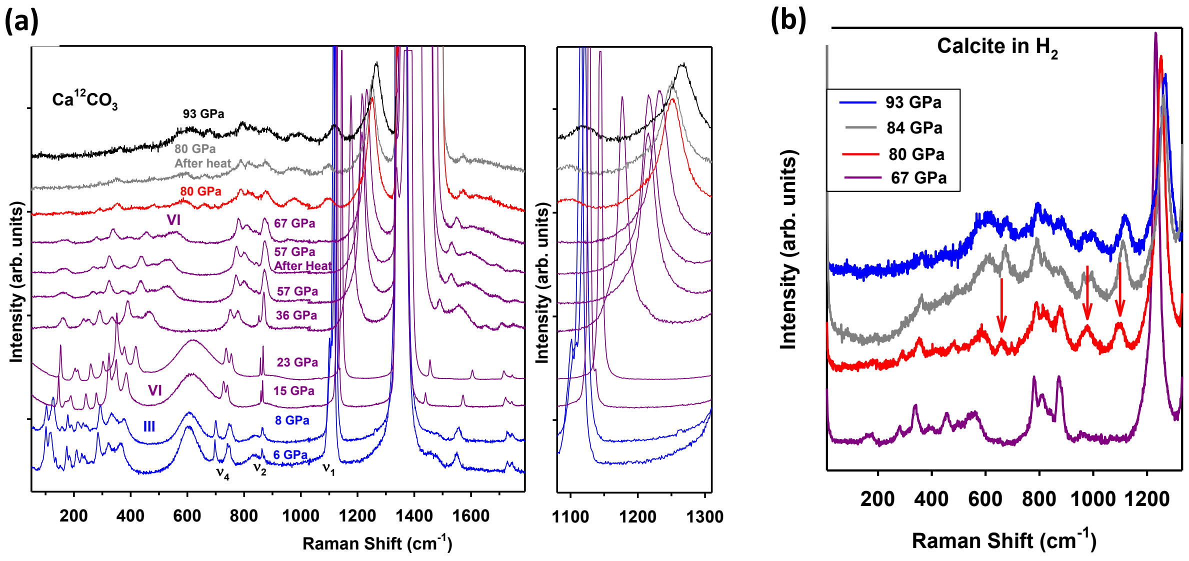

Figure 4. Raman spectra of Ca^{12}CO$_3$ in an H_2 medium measured on pressure increase. (a) The phase assignment (calcite III and calcite VI) is based on similarity of the low-frequency modes of calcite with the results of the previous experiments (Bayarjargal et al., 2018; Fong and Nicol, 1971). (b) Close up of the high-pressure spectra where a series of new Raman bands appears at 80 GPa (marked by arrows). The excitation wavelength is 488 nm.

The Raman spectra measured in a powder sample up to 93 GPa (Fig. 4(a)) showed that there is a good correspondence of the measured Raman spectra of calcite to those previously reported up to 45 GPa (Bayarjargal et al., 2018; Farsang et al., 2018; Fong and Nicol, 1971; Liu and Mernagh, 1990). At 6–8 GPa, the Raman spectra are consistent with calcite III (Fong and Nicol, 1971), while above 15 GPa the spectra indicate that calcite is in phase VI (Bayarjargal et al., 2018). Pulsed microsecond laser heating at 55 and 76 GPa did not change the XRD patterns and Raman spectra. However, above 80 GPa, the Raman peaks broaden and weaken, and new peaks appear (Fig. 4(b)) demonstrating the appearance of new bonding schemes.

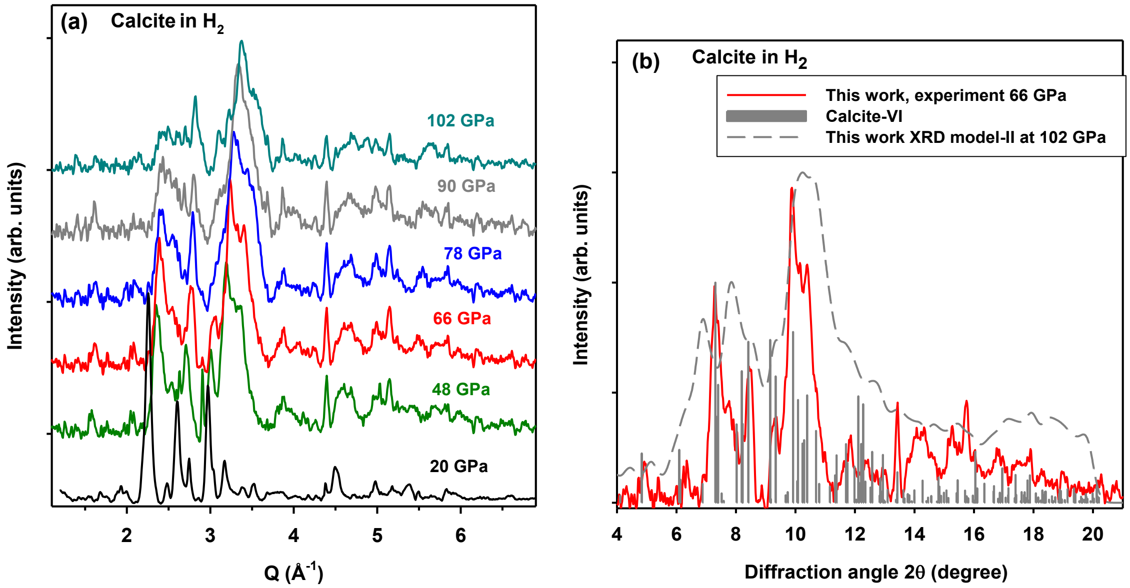

Figure 5. XRD pattern of Ca^{13}CO$_3$ in H_2 measured up to 102 GPa (a) and at 66 GPa (b). Solid red line in (b) is the experiment. Vertical bars correspond to the calculated XRD peaks of *P*-1 calcite VI (Merlini et al., 2012) structure. The lattice parameters of this structure (*a*=3.14(4) Å, *b*=4.71(4) Å, *c*=5.41(4) Å) were approximately adjusted to match the positions of the strongest experimental XRD features (the angles were fixed α=103.30°, β=94.73°, γ=89.21° using the values from (Merlini et al., 2012) at 30.4 GPa). Dashed grey line is the theoretically calculated XRD pattern calculated using Model-II (see text). The X-ray wavelength used was 0.3344 Å except for the pattern at 20 GPa, which was 0.2952 Å.

XRD powder diffraction measured up to 102 GPa demonstrated broadening and weakening of the Bragg peaks above 48 GPa (Fig. 5), which makes it difficult for definitive structural identification. However, we find a reasonably good match with the *P*-1 calcite VI of Ref. (Merlini et al., 2012) (Fig. 5 (b)). The lattice parameters and volumes (Figs. 6, 7) determined in this procedure were used to evaluate the hydrogenation content in powdered samples. The effects of hydrogenation on the lattice parameters is moderate based on the volume expansion determined in our single-crystal study below 24 GPa and the difference in the volume vs pressure curves measured here in hydrogenated powdered calcite and hydrogen-free calcite of Ref. (Merlini et al., 2012) (Fig. 6(b)). In the case of our powder diffraction data, the effect is within the experimental uncertainty.

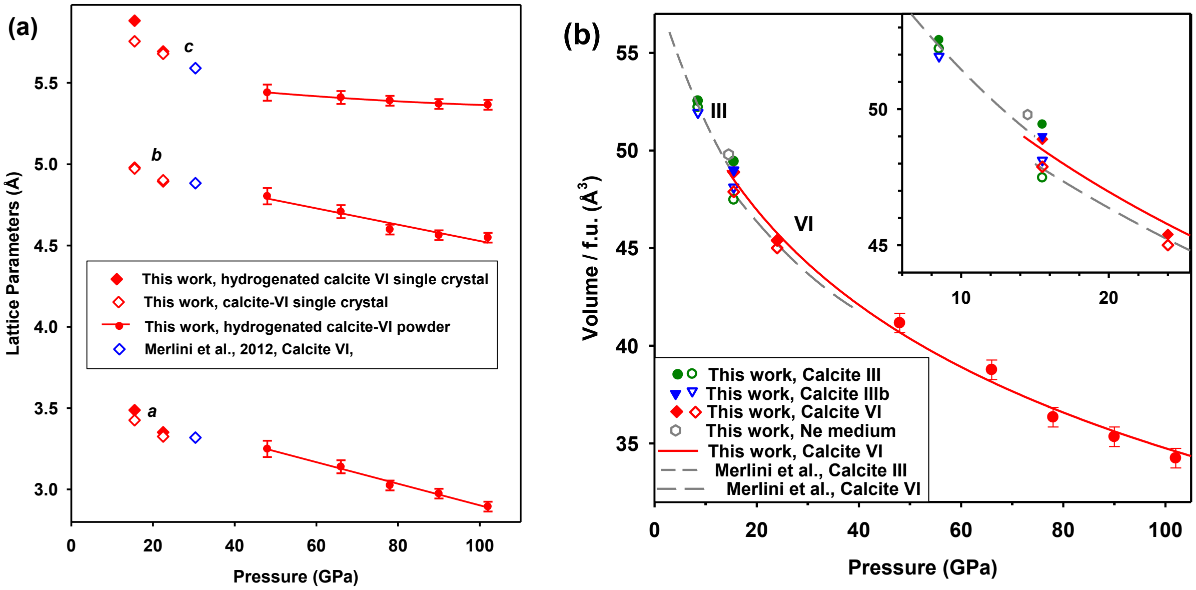

Figure 6. The lattice parameters (a) and volumes (b) of $CaCO_3$ as a function of pressure determined in experiments at room temperature. Symbols correspond to measurements in various calcite structures. Filled symbols correspond to hydrogenated materials. Solid lines through these data are guides to the eye in (a) and the Birch -Murnaghan equation of state (P_0=15 GPa, V_0=48.8 Å^3, K_0=128 GPa, K_0'=4.0) in (b). Red filled circles show the results of our analysis of powder XRD data of $Ca^{13}CO_3$ in H_2 assuming the calcite VI structure and the pressure independent unit cell angles. The uncertainties in the lattice parameters and the volumes are estimated by the quality of the fit based on this approximation. The results of previous experiment in *P*-1 calcite VI (Merlini et al., 2012) are presented for comparison. Dashed grey lines correspond to the volume vs pressure

curves measured in Ref. (Merlini et al., 2012) for calcite-III and calcite-VI. The inset shows an expanded view near 15 GPa.

The lattice expansion due to hydrogenation varies for different types of samples (single-crystal vs powder), phase, and pressure (Fig. 7). The value of the lattice expansion is a fraction of that expected empirically for incorporation of one H atom per formular unit from the EOS of atomic and molecular hydrogen (Loubeyre et al., 1996; Pépin et al., 2017). The latter values are in fair agreement with the volume expansion determined in our theoretical models (see below), with two H atoms incorporated per $CaCO_3$ unit.

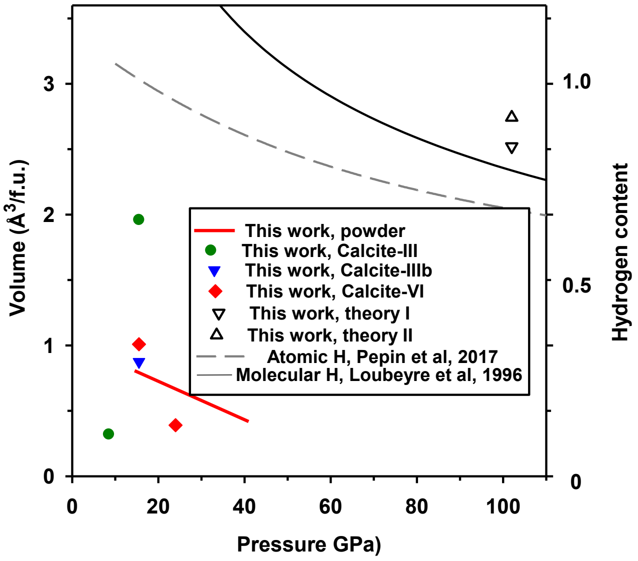

Figure 7. The volume expansion (per formula unit) due to hydrogenation of $CaCO_3$ as a function of pressure compared to the atomic volumes of hydrogen atoms. The volume expansion in single crystals is referenced to the nonhydrogenated crystals in the same point of observation. In powder samples, we determined it with respect to the volume vs pressure curves measured in Ref. (Merlini et al., 2012) in calcite-VI. The right axis shows an approximate hydrogen content in the pressure

range of measurements (scaled at 15 GPa). The experimental data in single-crystal (filled symbols) and powder (solid red line) are compared to the equations of state of molecular crystalline H_2 and in atomic hydrogen (volumes per hydrogen atom) taken from Refs. (Loubeyre et al., 1996; Pépin et al., 2017), respectively. Also, the results of theoretical calculations of this work in post-aragonite structure (Yao et al., 2018) are shown with open triangles for the two models described in the text referenced to the results of calculations in hydrogen-free crystals.

Raman spectroscopy below 67 GPa is consistent with calcite-VI (Fig. 4). However, this interpretation is not unique due to the hydrogenated nature of calcite, which is clearly manifested by the presence of the C(O)-H stretch and C(O)-H bend modes (Fig. 2). The presence of hydrogen attached to the carbonate CO_3 group adds extra vibrational modes and changes the crystal chemistry and symmetry thus affecting the vibrational frequencies and the Raman selection rules. It is worth noting that the association of two hydrogens to carbonate produces carbonic acid, which has the Raman frequencies similar to those observed here (Fig. 2) (Kohl et al., 2009). However, due to a relatively small hydrogenation, the Raman spectra below 67 GPa remain mainly that of anhydrous calcite-VI apart from the extra modes associated with the vibrations of hydrogens (Figs. 1, 2).

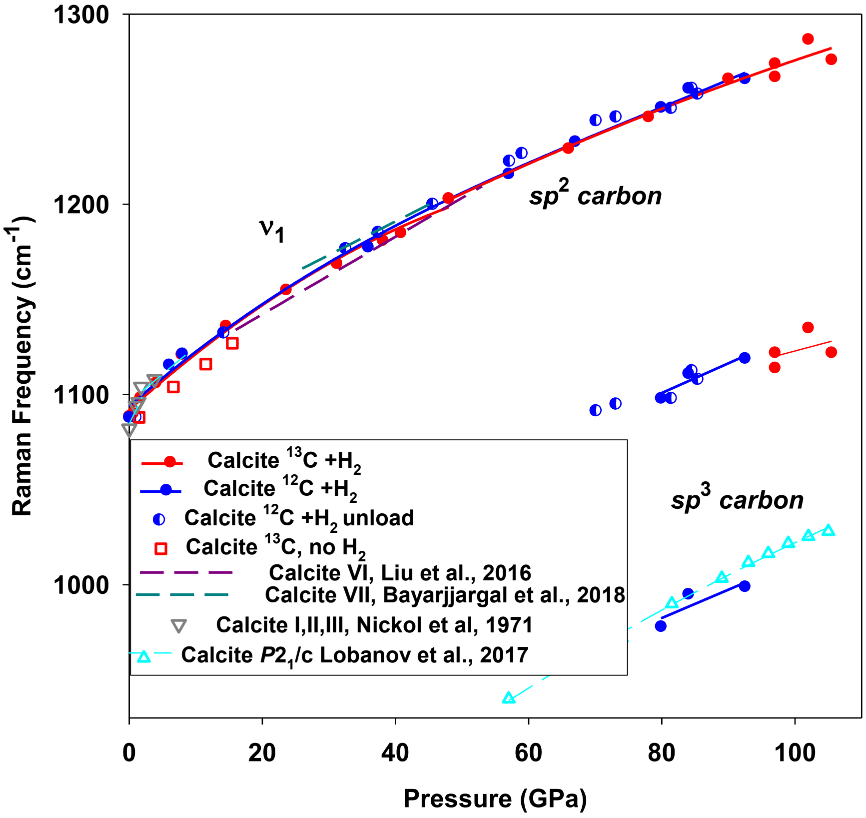

Figure 8. Raman frequencies of the C-O stretch mode of calcite as a function of pressure. The data for hydrogenated calcite of this work are presented by the filled and semi-filled circles. Open squares are from the control experiment with no medium. The results of previous experiments are shown by dashed lines and open symbols (Bayarjargal et al., 2018; Fong and Nicol, 1971; Liu and Mernagh, 1990; Lobanov et al., 2017).

sp^3 HYBRIDIZATION

The Raman peaks broaden and weaken above 67 GPa suggesting that a structural disorder occurs. Above 80 GPa new vibrational modes appear (Figs. 4(b), 8). The position of one of the newly appearing bands correlates well with that of the C-O stretch mode of $P2_1$/c calcite with sp^3 bonded carbon (Lobanov et al., 2017) (Fig. 8). The major Raman peak of $P2_1$/c calcite is the symmetric breathing mode of oxygen atoms in CO_4 tetrahedra, which form at the transformation. The second strong band at 1100 cm^{-1}, which appears in hydrogenated calcite above 80 GPa (Figs. 4(b), 8) must also originate from the C-O vibrations, but with an intermediate between sp^3 and sp^2 carbon hybridization patterns, for example, in the lattice where sp^2 bonded CO_3 groups are getting linked as in a transition state TS_3 of Ref. (Lobanov et al., 2017). It is important to note that such an intermediate state has not been detected in anhydrous calcite (Lobanov et al., 2017), while such states have been theoretically predicted in hydrogenated material (Kuang and Tse, 2022). The third new band recorded in hydrogenated calcite at 700 cm^{-1} (Fig. 4(b)) is close in frequency to the second strongest Raman mode of anhydrous calcite. Overall, our Raman observations at 80 GPa demonstrate a gradual transformation to the state sp^3 hybridized state in hydrogenated calcite at substantially lower pressure than in anhydrous calcite (105 GPa), where no sp^2 -sp^3 transformation was not found below 105 GPa even after the temperature annealing.

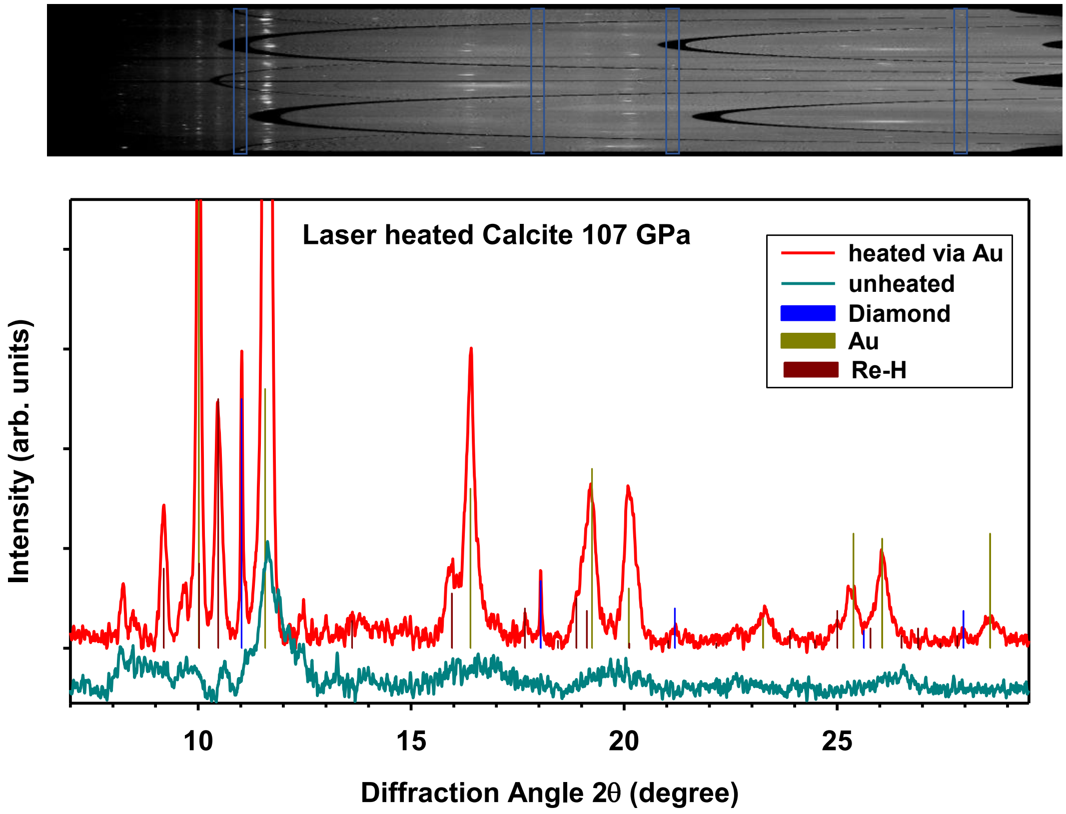

Figure 9. XRD patterns of $Ca^{13}CO_3$ in H_2 at 107 GPa. The top curve is taken near the laser heated position, while the bottom pattern is taken in the unheated area close to the center of the high-pressure cavity. Ticks correspond to Bragg peaks of the fitted phases. Calcite is represented by broad peaks (see the bottom curve), the strongest of which is at 11.7°; no structural information can be deduced from this information. The top panel is a 2D image of the heated area in rectangular coordinates. Blue rectangles frame single-crystal like diffraction peaks of diamond. The X-ray wavelength was 0.3738 Ǻ.

DIAMOND FORMATION

Increasing pressure beyond 80 GPa further broadens the Raman spectra and leads to the disappearance of weaker peaks. XRD measurements above 100 GPa show very broad peaks which are not suitable for analysis (Fig. 9). Laser heating of hydrogenated calcite up to 2700 K at these conditions via coupling to Au pieces did not result in the improvement of crystallinity of calcite (cf. (Lobanov et al., 2017)). However, we find that diamond crystallized (Fig. 9) in the form of tiny crystallites near the heated spot. At least four peaks have been used to identify the diamond structure; the fitted lattice parameter (3.372(1) Ǻ) shows a good agreement with the diamond EOS (Aleksandrov et al., 1987; Occelli et al., 2003).

The diamond synthesis from calcite at megabar pressure has been verified by performing Raman spectroscopy measurements of sample quenched to the ambient pressure. We used calcite with ^{13}C isotope to rule out that diamond is crystallized due to carbon transport from diamond anvils (Prakapenka et al., 2003) and to make sure that that the Raman signal from the synthesized ^{13}C diamond (Chrenko, 1988) is evidently spectrally separated from the diamond anvils. The Raman spectrum recorded on the recovered sample, which resides on one of the anvils in the sample cavity clearly demonstrates the signal of ^{13}C diamond (Fig. 10).

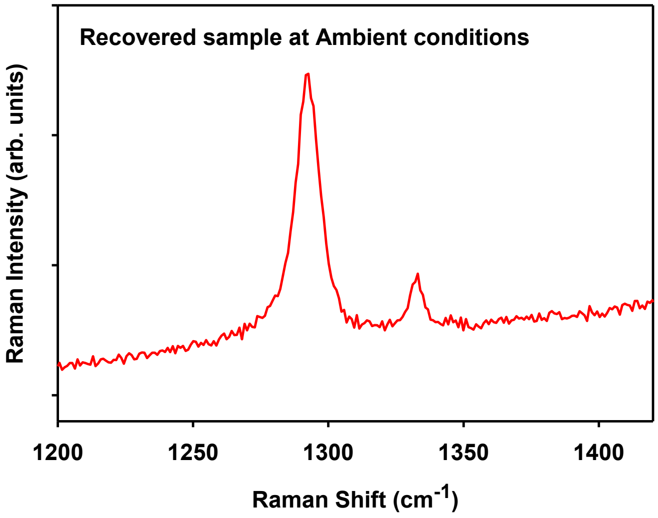

Figure 10. Raman spectra of diamond synthesis from $Ca^{13}CO_3$ calcite at 107 GPa. The peak at 1292 cm^{-1} is due to the synthesized ^{13}C diamond, while that at 1333 cm^{-1} is a background signal from the diamond anvil at which the sample resides after recovering to ambient conditions. The excitation wavelength is 488 nm.

THEORETICAL MODELS

Three $CaCO_3$ model structures with different initial H positions and content were used in the simulation. They are all based on a post-aragonite structure with 2 $CaCO_3$ formular units in the unit cell. Model-I started with 4 H atoms attached to C atoms, which are positioned above and below the carbonate ion plane. Model-II had 4 H atoms attached to O atoms in the carbonate plane. Model-III was hydrogen-rich, where 8 H_2 molecules were incorporated in the lattice. The structures were optimized at 48, 66, 78, 90, and 102 GPa.

The optimized structures have atomic H in Model-I and contain H_2 molecules in Model-II and Model-III. These structures are the same up to 90 GPa in all models except in Model-III, where H-CO_3-H, O-CH_2-OH, OH^- species form at 102 GPa. The optimized structures were expanded to 2x2x2 and 3x3x3 superstructures and then FPMD calculations were performed at 102 GPa and 1500 K for 20000 fs using isothermal-isobaric ensemble (NPT) ensemble.

The C-H and O-H bonds were observed to form associated with the creation of corner-shared C-O polyhedra, usually consisting of 2 or 3 CO_3 clusters (Fig. 11). We find transient H_2O molecules for about 4500 fs in Model-I, while many H_2O molecules form in Model-III. Molecular H_2 formed in Model-II and Model-III. Longer C-O corner-shared polyhedra exist in simulations of Model-II compared to Model-I, while C-C bonds and associated chains formed in Model-III but not in Model-I and Model-II.

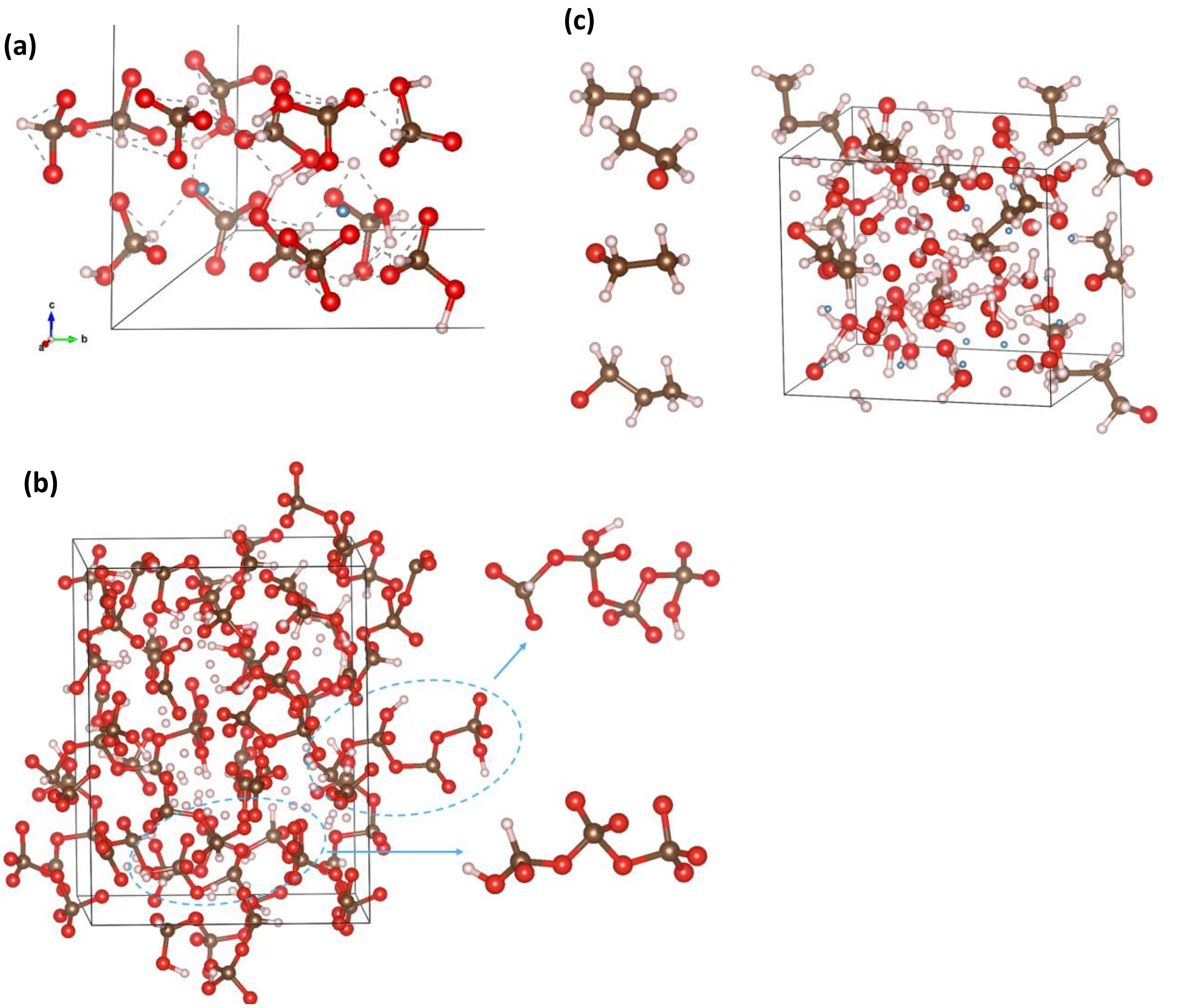

Figure 11. Snapshots of crystal structures of Model-I (a), Model-II (b), and Model-III (c) from FPMD simulations.

Fourier transform of the atomic position autocorrelation functions provides information about the vibrational frequencies, which can be compared to the experiments (Fig. 12). The C-O bonds exhibit vibrational frequencies at near 1200 cm^{-1} (Model-I) which is consistent with the stretching frequencies of C-O bands at 1000-1250 cm^{-1}, observed on Raman experiments (Fig. 4(b)). All models demonstrate the vibrational frequencies near 3200 cm^{-1}, corresponding to C-H and O-H

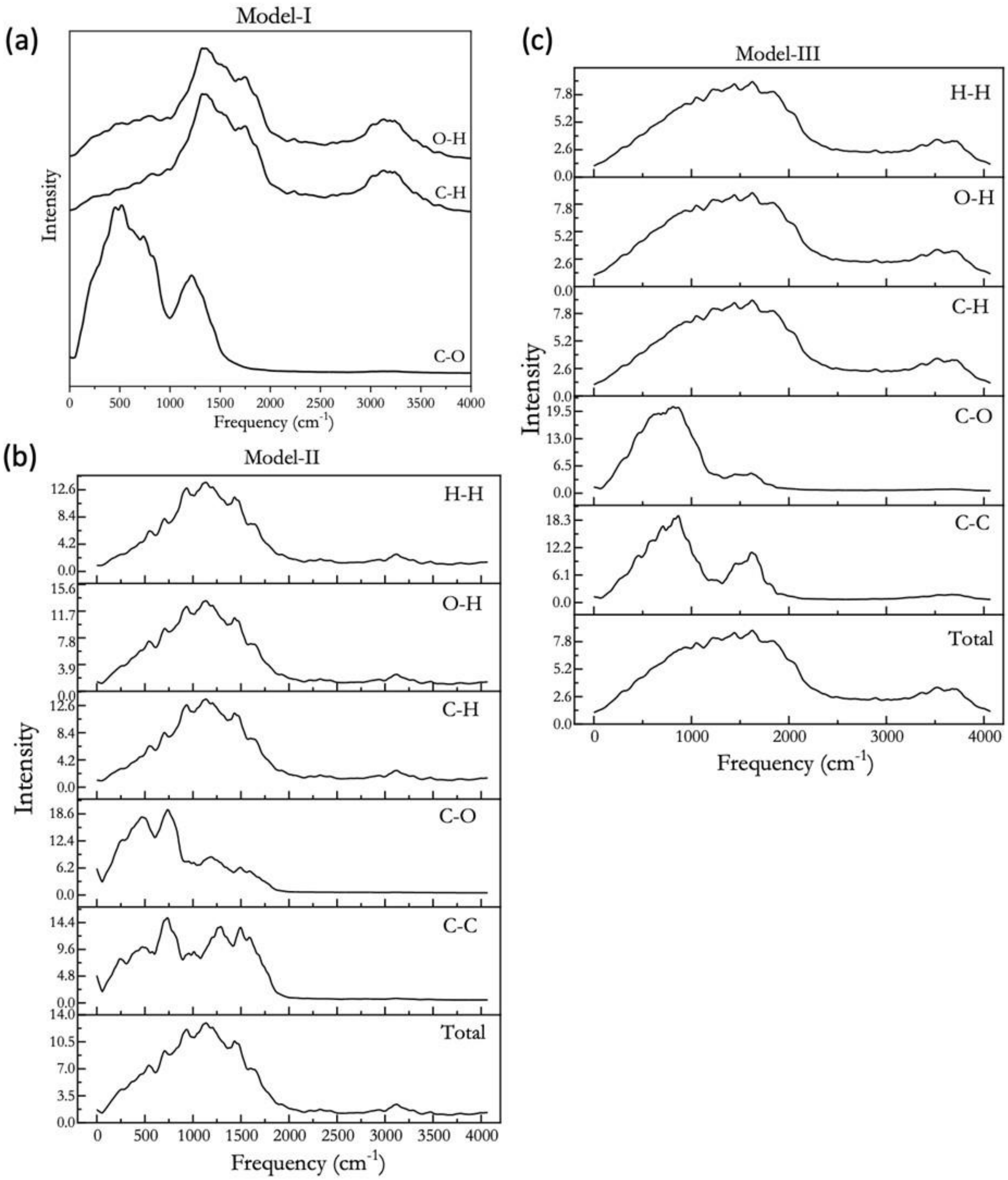

Figure 12. Power spectra computed from the Fourier transformation of different atomic distance autocorrelation functions in Model-I (a), Model-II (b), and Model-III (c). See Supplementary materials for the corresponding CONTCAR files.

stretching vibrations, while the peaks at 1300 cm^{-1} indicated the bending modes. The curves of C-H and O-H are almost identical, suggesting that the vibrations of O-H and C-H are highly correlated. These results correlate well with our Raman experiments, which demonstrate new peaks in hydrogenated calcite (Figs. 1, 2). Finally, the calculated XRD patterns, which are very similar for all models, are broadly consistent with the experiments (Fig. 5) even though the underlying theoretical structure (post-aragonite) is slightly different from that inferred experimentally (calcite VI). Our Raman experiments in the laser heated samples above 80 GPa did not show any sign of molecular H_2, which suggests that hydrogen was in atomic forms, thus, suggesting that Model-I is the best for describing the experimental data. Moreover, this is supported by the fact that our Raman experiments did not show any sign of H_2O related bands in the pressure range below 40 GPa, where the lattice modes and O-H stretch modes could be observed (Goncharov et al., 1999). Model-I and Model-II seem more relevant also because the experiments suggest low levels of hydrogenation (Fig. 7). Nevertheless, the modeling result suggests that the formation of C-C bonds is favored for high levels of hydrogenation (Model-III) and also stimulated by high pressures above 110 GPa (Kuang and Tse, 2022).

DISCUSSION

Calcite is one of the primary carbonate phases which enters the Earth's interior via subduction of oceanic crust. Our results demonstrate that hydrogen can be readily incorporated into its crystal structure at pressures above 0.5 GPa, and the interaction of hydrogen with the host lattice is largely driven by interactions between H and the C-O network. Consequently, these mechanisms of incorporation can be generalized to other carbonate systems as well. It has been shown that Ca-bearing carbonates undergo substitution reactions to form (Mg,Fe) carbonates and Ca-rich fluids at 1-3 GPa and high temperatures along the P-T pathways of subducting slabs (Chen et al., 2023; Poli et al., 2009). All of these carbonates adopt similar C-O structural motifs below 70-80 GPa, involving different arrangements of tetrahedrally coordinated Ca, Mg and Fe cations (Merlini et al., 2012). As a result, nominally anhydrous carbonates will likely incorporate small quantities of hydrogen at depth, enhancing the hydrogen storage capacity of subducting slabs at conditions where carbonates are stable in the presence of reduced C-O-H fluids (Kadik, 2006; Weidendorfer et al., 2020). The present results suggest that carbonates can store up to 5000 ppm H, when using the molar weight and hydrogenation level of $CaCO_3$ determined here. This result differs from experimental studies of the H_2O-$CaCO_3$ system at 1-12 GPa and up to 673 K (Zhao et al., 2022) where no reaction is observed, indicating that redox conditions play a role in the hydrogen storage capacity of $CaCO_3$ although further study is needed on the H_2-$CaCO_3$ system at mantle temperatures.

Mg,Fe-carbonates can be petrologically stable in the lower mantle (Dorfman et al., 2018), and recent work indicates that these phases react with Ca-silicate perovskite to form calcite and bridgmanite at pressures above 70 GPa and high temperatures (Lv et al., 2021). Previous studies have demonstrated that hydrogenation occurs when metallic iron is present in hydrous environments extending from the conditions of the mantle transition zone to those of the core-mantle boundary (Kim et al., 2023; Zhu et al., 2019)). Our results demonstrate that these hydrogenated, reducing environments may result in carbonate decomposition. Consequently, calcite formation in the deep lower mantle is more favorable under oxidizing or anhydrous conditions.

CONCLUSIONS

Experiments and theory in the present study show that calcite hydrogenates in a H_2 medium at high pressures starting from as low as <0.5 GPa. Calcite accepts up to 1 H atom per formula unit depending on pressure, sample form (single-crystal or powder), and time. Hydrogenated calcite under pressure below 40 GPa shows the same phase transition sequence as anhydrous calcite. Above 40 GPa XRD and Raman features broaden, but the structural behavior is consistent with calcite residing in phase VI. Above 80 GPa, new Raman features appear signaling chemical or phase transformations in the C-O bonding scheme. Above 107 GPa, we find that heating results in the formation of diamond. This behavior is in good accord with theoretical FPMD modeling, which shows the formation of corner-shared C-O polyhedra and C-C bonds in the limit of high pressures and high H concentration.

ACKNOWLEDGEMENT

Parts of this research were carried out at the GeoSoilEnviroCARS (The University of Chicago, Sector 13), Advanced Photon Source (Argonne National Laboratory). GeoSoilEnviroCARS is supported by the National Science Foundation—Earth Sciences (No. EAR-1634415). Use of the GSECARS Raman System was supported by the NSF MRI Proposal (No. EAR-1531583). Portions of this work were performed at HPCAT (sector 16) of the Advanced Photon Source (APS), Argonne National Laboratory. HPCAT operations are supported by DOE-NNSA's Office of Experimental Sciences. The Advanced Photon Source is a U.S. Department of Energy (DOE) Office of Science User Facility operated for the DOE Office of Science by Argonne National Laboratory under Contract No. DE-AC02-06CH11357**.** We acknowledge DESY (Hamburg, Germany), a member of the Helmholtz Association HGF, for the provision of experimental facilities. Parts of this research were carried out at Petra III (beamline P02.2). Beamtime was allocated for proposals I-20221160 and I-20230233. A.F.G. acknowledges the support of NSF CHE 2302437. A.F.G. and J.S.T. acknowledge the support of Carnegie Canada. M.B. acknowledges the support of Deutsche Forschungsgemeinschaft (DFG Emmy-Noether Program project BY112/2-1). J.S.T. wishes to thank NSERC for a Discovery Grant.

Aleksandrov, I.V., Goncharov, A.F., Zisman, A.N., Stishov, S.M., 1987. Diamond at high pressures - Raman scattering of light, equation of state, and a high pressure scale. Zhurnal Eksperimentalnoi i Teoreticheskoi Fiziki 93, 680-691.

Bali, E., Audétat, A., Keppler, H., 2013. Water and hydrogen are immiscible in Earth's mantle. Nature 495, 220-222.

Bayarjargal, L., Fruhner, C.J., Schrodt, N., Winkler, B., 2018. $CaCO_3$ phase diagram studied with Raman spectroscopy at pressures up to 50 GPa and high temperatures and DFT modeling. Physics of the Earth and Planetary Interiors 281, 31-45.

Bykov, M., Bykova, E., Pickard, C.J., Martinez-Canales, M., Glazyrin, K., Smith, J.S., Goncharov, A.F., 2021. Structural and vibrational properties of methane up to 71 GPa. Physical Review B 104, 184105.

Catalli, K., Williams, Q., 2005. Letter: A high-pressure phase transition of calcite-III. American Mineralogist 90, 1679-1682.

Chen, C., Förster, M.W., Foley, S.F., Shcheka, S.S., 2023. Carbonate-rich crust subduction drives the deep carbon and chlorine cycles. Nature 620, 576-581.

Chrenko, R.M., 1988. ^{13}C-doped diamond: Raman spectra. Journal of Applied Physics 63, 5873-5875.

Dorfman, S.M., Badro, J., Nabiei, F., Prakapenka, V.B., Cantoni, M., Gillet, P., 2018. Carbonate stability in the reduced lower mantle. Earth and Planetary Science Letters 489, 84-91.

Farsang, S., Facq, S., Redfern, S.A.T., 2018. Raman modes of carbonate minerals as pressure and temperature gauges up to 6 GPa and 500 °C. American Mineralogist 103, 1988-1998.

Fong, M.Y., Nicol, M., 1971. Raman Spectrum of Calcium Carbonate at High Pressures. The Journal of Chemical Physics 54, 579-585.

Gavryushkin, P.N., Martirosyan, N.S., Inerbaev, T.M., Popov, Z.I., Rashchenko, S.V., Likhacheva, A.Y., Lobanov, S.S., Goncharov, A.F., Prakapenka, V.B., Litasov, K.D., 2017. Aragonite-II and $CaCO_3$-VII: New High-Pressure, High-Temperature Polymorphs of $CaCO_3$. Crystal Growth & Design 17, 6291-6296.

Goncharov, A.F., Prakapenka, V.B., Struzhkin, V.V., Kantor, I., Rivers, M.L., Dalton, D.A., 2010. X-ray diffraction in the pulsed laser heated diamond anvil cell. Review of Scientific Instruments 81.

Goncharov, A.F., Struzhkin, V.V., Mao, H.-k., Hemley, R.J., 1999. Raman Spectroscopy of Dense H_2O and the Transition to Symmetric Hydrogen Bonds. Physical Review Letters 83, 1998-2001.

Holtgrewe, N., Greenberg, E., Prescher, C., Prakapenka, V.B., Goncharov, A.F., 2019. Advanced integrated optical spectroscopy system for diamond anvil cell studies at GSECARS. High Pressure Research 39, 457-470.

Kadik, A.A., 2006. Oxygen fugacity regime in the upper mantle as a reflection of the chemical differentiation of planetary materials. Geochemistry International 44, 56-71.

Kim, T., O'Rourke, J.G., Lee, J., Chariton, S., Prakapenka, V., Husband, R.J., Giordano, N., Liermann, H.-P., Shim, S.-H., Lee, Y., 2023. A hydrogen-enriched layer in the topmost outer core sourced from deeply subducted water. Nature Geoscience 16, 1208-1214.

Kohl, I., Winkel, K., Bauer, M., Liedl, K.R., Loerting, T., Mayer, E., 2009. Raman Spectroscopic Study of the Phase Transition of Amorphous to Crystalline β-Carbonic Acid. Angewandte Chemie International Edition 48, 2690-2694.

Kuang, H., Tse, J.S., 2022. High-Temperature, High-Pressure Reactions of H_2 with $CaCO_3$ Melts. Physica Status Solidi (b) 259, 2100644.

Liu, J., Caracas, R., Fan, D., Bobocioiu, E., Zhang, D., Mao, W.L., 2016. High-pressure compressibility and vibrational properties of $(Ca,Mn)CO_3$. American Mineralogist 101, 2723-2730.

Liu, L.-G., Mernagh, T.P., 1990. Phase transitions and Raman spectra of calcite at high pressures and room temperature. American Mineralogist 75, 801-806.

Lobanov, S.S., Chen, P.-N., Chen, X.-J., Zha, C.-S., Litasov, K.D., Mao, H.-K., Goncharov, A.F., 2013. Carbon precipitation from heavy hydrocarbon fluid in deep planetary interiors. Nature Communications 4, 2446.

Lobanov, S.S., Dong, X., Martirosyan, N.S., Samtsevich, A.I., Stevanovic, V., Gavryushkin, P.N., Litasov, K.D., Greenberg, E., Prakapenka, V.B., Oganov, A.R., Goncharov, A.F., 2017. Raman spectroscopy and x-ray diffraction of $CaCO_3$ at lower mantle pressures. Physical Review B 96, 104101.

Loubeyre, P., LeToullec, R., Hausermann, D., Hanfland, M., Hemley, R.J., Mao, H.K., Finger, L.W., 1996. X-ray diffraction and equation of state of hydrogen at megabar pressures. Nature 383, 702-704.

Lv, M., Dorfman, S.M., Badro, J., Borensztajn, S., Greenberg, E., Prakapenka, V.B., 2021. Reversal of carbonate-silicate cation exchange in cold slabs in Earth's lower mantle. Nature Communications 12, 1712.

Merlini, M., Hanfland, M., Crichton, W.A., 2012. $CaCO_3$-III and $CaCO_3$-VI, high-pressure polymorphs of calcite: Possible host structures for carbon in the Earth's mantle. Earth and Planetary Science Letters 333-334, 265-271.

Mezouar, M., Giampaoli, R., Garbarino, G., Kantor, I., Dewaele, A., Weck, G., Boccato, S., Svitlyk, V., Rosa, A.D., Torchio, R., Mathon, O., Hignette, O., Bauchau, S., 2017. Methodology for in situ synchrotron X-ray studies in the laser-heated diamond anvil cell. High Pressure Research 37, 170-180.

Occelli, F., Loubeyre, P., LeToullec, R., 2003. Properties of diamond under hydrostatic pressures up to 140 GPa. Nature Materials 2, 151-154.

Oganov, A.R., Glass, C.W., Ono, S., 2006. High-pressure phases of $CaCO_3$: Crystal structure prediction and experiment. Earth and Planetary Science Letters 241, 95-103.

Ono, S., Kikegawa, T., Ohishi, Y., 2007. High-pressure transition of CaCO3. American Mineralogist 92, 1246-1249.

Ono, S., Kikegawa, T., Ohishi, Y., Tsuchiya, J., 2005. Post-aragonite phase transformation in $CaCO_3$ at 40 GPa. American Mineralogist 90, 667-671.

Pennacchioni, L., Speziale, S., Winkler, B., 2023. Elasticity of natural aragonite samples by Brillouin spectroscopy. Physics and Chemistry of Minerals 50, 22.

Pépin, C.M., Geneste, G., Dewaele, A., Mezouar, M., Loubeyre, P., 2017. Synthesis of $FeH_{5:}$ A layered structure with atomic hydrogen slabs. Science 357, 382-385.

Pickard, C.J., Needs, R.J., 2015. Structures and stability of calcium and magnesium carbonates at mantle pressures. Physical Review B 91, 104101.

Poli, S., Franzolin, E., Fumagalli, P., Crottini, A., 2009. The transport of carbon and hydrogen in subducted oceanic crust: An experimental study to 5 GPa. Earth and Planetary Science Letters 278, 350-360.

Poli, S., Schmidt, M.W., 2002. Petrology of Subducted Slabs. Annual Review of Earth and Planetary Sciences 30, 207-235.

Prakapenka, V.B., Kubo, A., Kuznetsov, A., Laskin, A., Shkurikhin, O., Dera, P., Rivers, M.L., Sutton, S.R., 2008. Advanced flat top laser heating system for high pressure research at GSECARS: application to the melting behavior of germanium. High Pressure Research 28, 225-235.

Prakapenka, V.B., Shen, G., Dubrovinsky, L.S., 2003. Carbon transport in diamond anvil cells. High Temperatures-high Pressures, 237-249.

Rapp, R.P., Watson, E.B., 1995. Dehydration Melting of Metabasalt at 8–32 kbar: Implications for Continental Growth and Crust-Mantle Recycling. Journal of Petrology 36, 891-931.

Schmidt, M.W., Poli, S., 2014. 4.19 - Devolatilization During Subduction, in: Holland, H.D., Turekian, K.K. (Eds.), Treatise on Geochemistry (Second Edition). Elsevier, Oxford, pp. 669-701.

Suito, K., Namba, J., Horikawa, T., Taniguchi, Y., Sakurai, N., Kobayashi, M., Onodera, A., Shimomura, O., Kikegawa, T., 2001. Phase relations of $CaCO_3$ at high pressure and high temperature. American Mineralogist 86, 997-1002.

Weidendorfer, D., Manning, C.E., Schmidt, M.W., 2020. Carbonate melts in the hydrous upper mantle. Contributions to Mineralogy and Petrology 175, 72.

Yao, X., Xie, C., Dong, X., Oganov, A.R., Zeng, Q., 2018. Novel high-pressure calcium carbonates. Physical Review B 98, 014108.

Zhao, X., Zheng, Z., Chen, J., Gao, Y., Sun, J., Hou, X., Xiong, M., Mei, S., 2022. High P-T Calcite-Aragonite Phase Transitions Under Hydrous and Anhydrous Conditions. Frontiers in Earth Science 10.

Zhu, F., Li, J., Liu, J., Dong, J., Liu, Z., 2019. Metallic iron limits silicate hydration in Earth's transition zone. Proceedings of the National Academy of Sciences 116, 22526-22530.